# Supplementary Information

**Preparation of single-crystal ternary cathode materials via recycling spent cathodes for high performance lithium-ion batteries**

Cheng Huang,[a] Xue Xia,[a] Ziwei Chi,[a] Zeheng Yang,*[a,c] Haijian Huang,[a,b] Zhangxian Chen,[a,b] Weijian Tang,[a,b] Guoqing Wu,[c] Huayong Chen,[c] and Weixin Zhang*[a,b]

[a] School of Chemistry and Chemical Engineering, Hefei University of Technology, Hefei, Anhui, 230009, PR China

[b] Institute of Energy, Hefei Comprehensive National Science Center, Hefei, Anhui, 230009, PR China

[c] Anhui Industrial Innovation Center of lithium Battery Green Recycling, Jieshou, Fuyang, Anhui, 236500, PR China

* Corresponding authors. Fax: 86−551−62901450

E-mail: zehengyang@hfut.edu.cn, wxzhang@hfut.edu.cn

Postal address: School of Chemistry and Chemical Engineering, Hefei University of Technology, No. 193 Tunxi Road, 230009 Hefei, Anhui, Chi

**Experimental Section**

*Chemicals and materials*:

$LiOH \cdot H_2O$ (AR, 95.0%), $LiNO_3$ (AR, 99.9%), $Li_2CO_3$ (AR, 98.0%), and NaCl (AR, 99.5%) were purchased from Sinopharm Chemical Reagent Co, Ltd and used without further purification. All the water used is de-ionized water. The spent NCM523 (denoted as S523), NCM622 (denoted as S622) cathode materials were collected from spent LIBs obtained from electronic market. The $Ni_{0.8}Co_{0.1}Mn_{0.1}(OH)_2$ precursor was prepared by referring to our previous work.[1] The co-precipitated $Ni_{0.8}Co_{0.1}Mn_{0.1}(OH)_2$ precursor was mixed with $Li_2CO_3$ with mass ratio of 1:0.435, followed by calcination in muffle furnace at 500 ℃ for 5 h, and then at 800 ℃ for 15 h to obtain the S811 product.

*Collection of spent cathode materials*:

In a typical collection, the spent LIBs were immersed in NaCl aqueous solution (0.01 M) to fully discharge. Next, the spent LIBs were dismantled manually to separate positive electrode, negative electrode and separator in a fume hood. The obtained positive electrode was then put into N-methyl-2-pyrrolidone (NMP) solvent with sonication to peel off spent cathode material from the current collector. After filtrating, washing with water, and drying, the spent cathode material powders were obtained.

*Crushing of spent cathode materials*:

To crush the large secondary particles in the spent cathode materials, the ball

milling method was employed. The spent cathode material powder was placed in a ball mill tank and ground at a rotating speed of 1000 r $min^{-1}$ for 3 h to get primary particles.

*Preparation of single-crystal NCM622 (denoted as SC622) from S622*:

Two different NCM622 powders, including the original particles collected from spent electrodes and the crushed particles were mixed respectively with the lithium molten salts (2:3 in molar ratio of LiOH:$LiNO_3$) at the molar ratio of 1:5.7 for NCM622 to lithium molten salts. The mixture was first calcined at 500 ℃ for 5 h, then at 850 ℃ for 11 h in air. After that, the mixture was allowed to cool down naturally. The final single-crystal particles were obtained after washing the superfluous lithium salts and annealing subsequently at 750 °C for 5 h in air. The corresponding SC622 samples regenerated from the collected original particles and the crushed particles are referred as SC622-1 and SC622-2, respectively.

Similarly, the ball milling method is also adopted to crush the S523 and S811 particles for regeneration. The regenerated single-crystal samples named as SC523 and SC811 were acquired following the same calcination procedure in the lithium molten salts, except that oxygen atmosphere was used for SC811.

*Co-regeneration of different waste NCM cathode materials for preparation of single-crystal $LiNi_xCo_yMn_zO_2$*:

Similar ball milling and calcination procedures in the Li-based molten salts were applied for preparation of the following single-crystal cathode materials from

different waste NCM cathode materials. Single-crystal $LiNi_{0.55}Co_{0.2}Mn_{0.25}O_2$ (SC55) was regenerated from equimolar amounts of S523 and S622. Single-crystal $LiNi_{0.65}Co_{0.15}Mn_{0.2}O_2$ (SC65) was regenerated from equimolar amounts of S523 and S811. Single-crystal $LiNi_{0.70}Co_{0.15}Mn_{0.15}O_2$ (SC70) was regenerated from equimolar amounts of S622 and S811. Single-crystal $LiNi_{0.633}Co_{0.167}Mn_{0.2}O_2$ (SC633) was regenerated from equimolar amounts of S523, S622 and S811.

*Preparation of single-crystal $LiNi_xCo_yMn_zO_2$ with a targeted Ni content of 80% from S523 or S622 materials:*

Firstly, ball milling was employed to crush S523 or S622 cathode materials with a rotating speed of 1000 r $min^{-1}$ for 3 h to get the corresponding primary particles.

To regenerate S523 into single-crystal $LiNi_{0.8}Co_{0.08}Mn_{0.12}O_2$, crushed S523, NiO, and lithium molten salts (LiOH-$LiNO_3$ with a molar ratio of 2:3) were mixed in a molar ratio of 0.4: 0.6: 5.7. To regenerate S622 into single-crystal $LiNi_{0.8}Co_{0.1}Mn_{0.1}O_2$, crushed S622, NiO, and lithium molten salts (LiOH-$LiNO_3$ with a molar ratio of 2:3) were mixed in a molar ratio of 0.5: 0.5: 5.7. The two different mixtures were first calcined at 500 ℃ for 5 h, then at 850 ℃ for 11 h in oxygen atmosphere. After that, the mixtures were allowed to cool down naturally. The final single-crystal $LiNi_{0.8}Co_{0.08}Mn_{0.12}O_2$ and single-crystal $LiNi_{0.8}Co_{0.1}Mn_{0.1}O_2$ were obtained after washing the superfluous lithium salts and annealing subsequently at 750 °C for 5 h in oxygen atmosphere.

*Material characterizations*:

The morphology of samples was characterized by field emission scanning

electron microscopy (FESEM, Hitachi SU8020). X-ray powder diffraction (XRD, PANalytical X-Pert PRO MPD X-ray diffractometer with Cu K$\alpha$ radiation source at 40 kV, $\lambda$=0.154178 nm) was applied to explore the structure of samples. Transmission electron microscopy (TEM) and high-resolution transmission electron microscopy (HRTEM) characterizations were both on a JEM-2100F instrument (JEOL Ltd, Japan). X-ray photoelectron spectroscopy (XPS) was conducted to detect the valence on a Thermo ESCALAB250Xi instrument.

*Electrochemical characterizations*:

The lithium storage properties of the samples were tested in coin-type (CR2032) cells. The electrodes were made by spreading the slurry which is composed of active material (80 wt%), acetylene black (10 wt%), and PVDF (polyvinylidene difluoride, 10 wt%) in NMP onto aluminum foil current collector and then dried in vacuum at 80 °C for 12 h. Afterward, the foil was punched into 12 mm disks to obtain the electrode film. The resulting electrode film was served as cathode, with a lithium metal plate as counter electrode, and Celgard 2400 membrane as the separator. The electrolyte solution is composed of 1 M $LiPF_6$ in mixture of ethyl methyl carbonate (EMC), dimethyl carbonate (DMC), and ethylene carbonate (EC) with 1:1:1 volume ratio. The coin-type cells were assembled in glove box and left standing for 24 h before measurements. Galvanostatic charge/discharge measurements were carried out at a current density of 1 C, and rate capacity measurement was performed at the current densities of 0.2 C, 0.5 C, 1 C, 2 C, 5 C, and 10 C using a cell test system (Neware Battery Test System, Shenzhen Neware Electronic Co, China) in the voltage range

between 2.8 V and 4.3 V (*vs*. $Li^+/Li$) at room temperature. Cyclic voltammetry (CV) measurement was also conducted in the voltage range of 2.8−4.3 V and at a scan rate of 0.2 mV $s^{-1}$ using a CHI-760E (Shanghai Chenhua Instrument Limited Corporation, China) electrochemical workstation. Electrochemical impedance spectroscopy (EIS) was performed on the same electrochemical workstation with an amplitude of 5 mV, and the frequency range of 0.01−100 kHz.

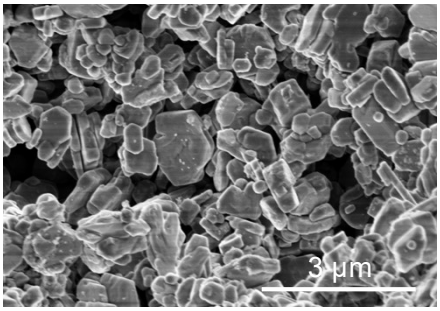


**Fig. S1.** FESEM image of SC622-1.

After directly regenerated in the molten salt system, the broken particles are converted into single-crystal particles (Fig. S1). These single-crystal particles exist in irregular plate-like structure but with serious agglomeration.

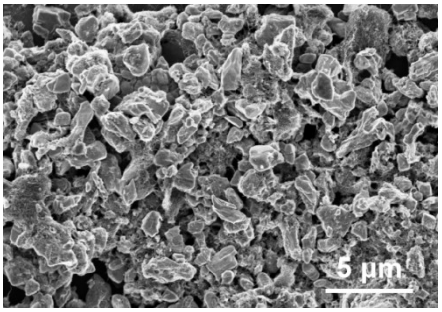


**Fig. S2.** FESEM image of S622 after crushing by ball milling method.

After ball milling, the large secondary particles of S622 are crushed into smaller primary ones**.**

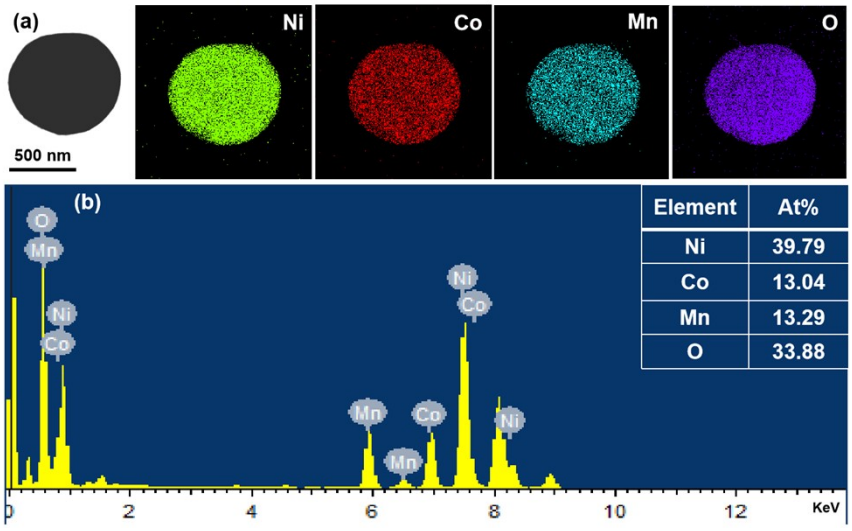


**Fig. S3.** (a) Element (Ni, Co, Mn, and O) mappings and (b) EDS spectrum of SC622-1.

The Ni, Co, Mn, and O are uniformly distributed in particles (Fig. S3a), and EDS results suggest that the stoichiometric ratio of Ni:Co:Mn is close to 6:2:2 (Fig. S3b), which is consistent with the molar ratio of the target product.

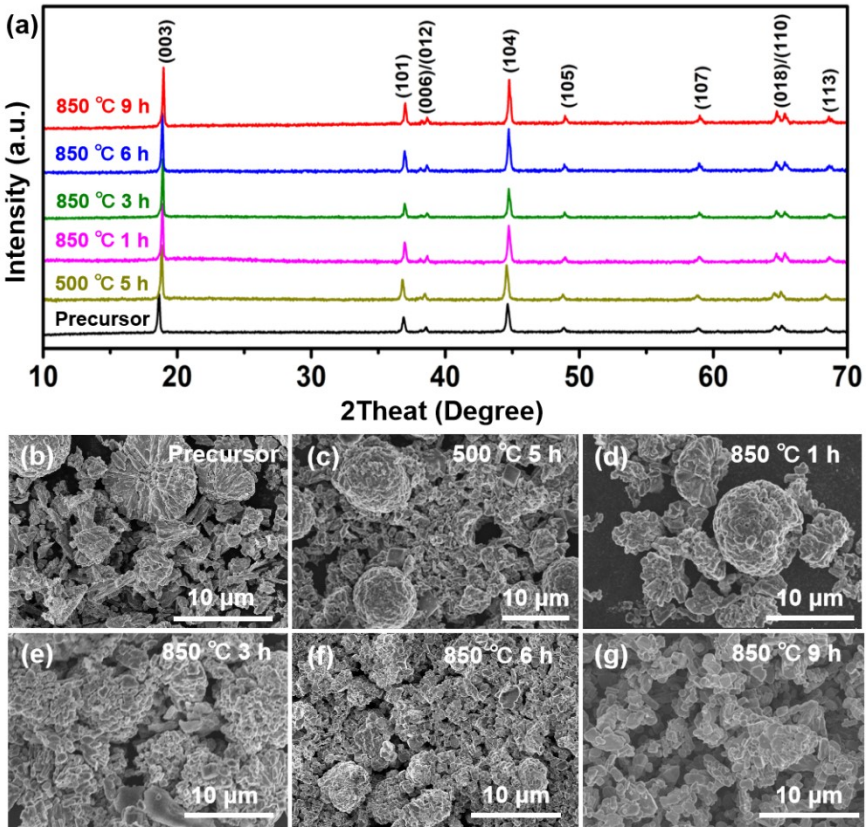


**Fig. S4.** The formation process of SC622-1 (a) *Ex-situ* XRD patterns. (b−g) *Ex-situ* FESEM images.

The *ex-situ* XRD and FESEM characterizations are utilized to explore the phase and morphology evolution during the high-temperature molten salt regeneration process. As shown in Fig. S4a, when the annealing temperature and time increase to 850 ℃ and 9 h, respectively, the XRD pattern can be still assigned to layered structure. From the morphological point of view, the S622 particles (Fig. S4b) are severely broken after the sample is heated at 850 ℃ for 3 h (Fig. S4c−e). As the annealing process continues for another 3 h, the individual particles are observed with increasing sizes (Fig. S4f), but still with plenty of large broken particles. After holding the temperature at 850 ℃ for 9 h (Fig. S4g), the large particles disintegrate but with agglomerated irregular particles.

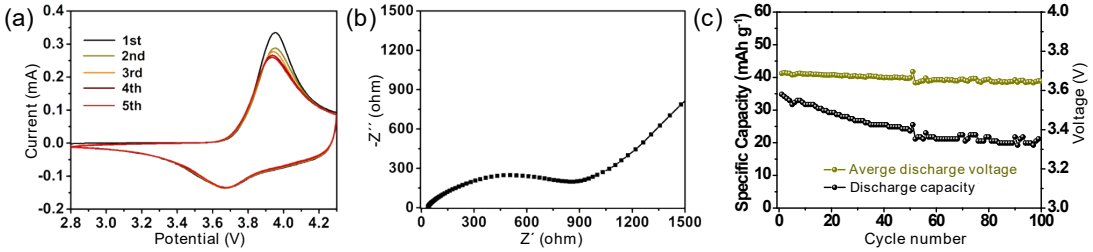


**Fig. S5.** (a) CV curves at a scan rate of 0.2 mV $s^{-1}$, (b) Nyquist plots, and (c) cycling performance and average discharge voltage of S622.

The anodic peak locates at 3.87 V and the cathodic peak at 3.66 V for S622 (Fig. S5a), while 3.70 V (the anodic peak) and 3.80 V (the cathodic peak) for these SC622 samples, uncovering the much smaller polarization for the regenerated SC622 samples. In addition, the S622 shows a larger $R_{ct}$ (Fig. S5b) than the SC622 samples, resulting in the poor electrochemical properties (Fig. S5c). The capacity of S622 is only 34.8 mAh $g^{-1}$ at 1 C and remains 21.1 mAh $g^{-1}$ after 100 cycles. The average discharge voltage of S622 is droped faster (Fig. S5c, from 3.687 V to 3.648V) within 100 cycles and lower than both of SC622 samples.

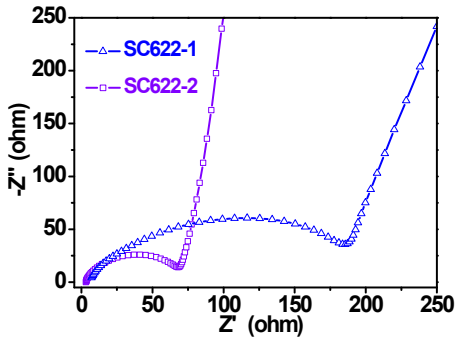


**Fig. S6.** Nyquist plots of the SC622-1 and SC622-2 samples.

The SC622-2 electrode shows the smaller $R_{ct}$ than SC622-1, pointing to a much lower SEI resistance and a faster $Li^+$ diffusion for SC622-2.

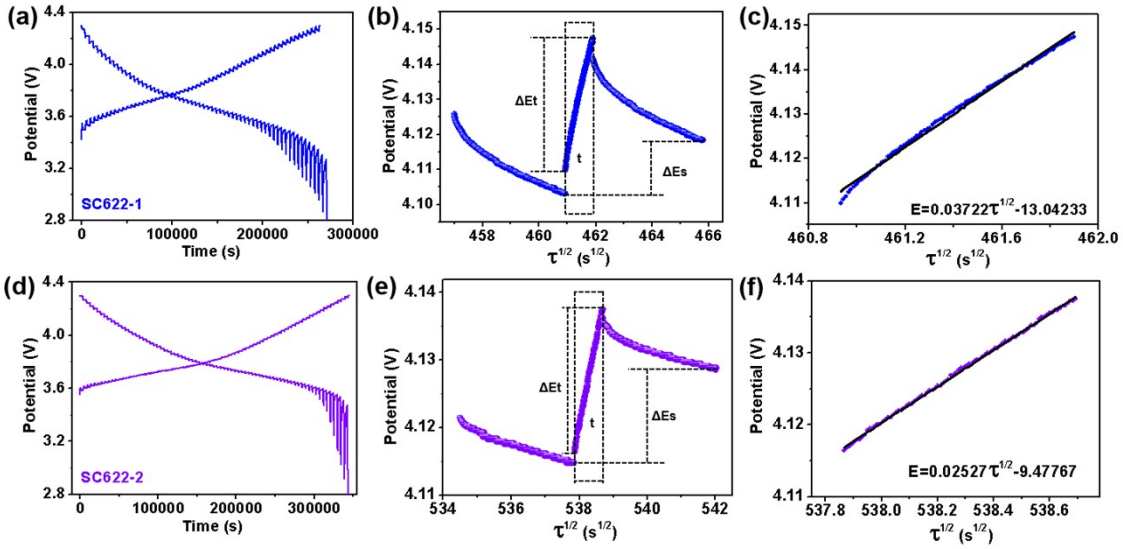


**Fig. S7.** (a, d) Charge-discharge voltage profiles, (b, e) enlarged galvanostatic titration curves during charge and (c, f) the linear correlation between the change in voltage against $\tau^{1/2}$ for SC622-1 and SC622-2, respectively.

GITT measurements were utilized to reveal the $Li^+$ diffusion kinetics in SC622. Fig. S7a and S7d showed the charge/discharge voltage profiles of SC622-1 and SC622-2, while the corresponding enlarged galvanostatic titration curves are displayed in Fig. S7b and S7e. Based on the linear correlation between the change in voltage against $\tau^{1/2}$ for SC622-1 and SC622-2 (Fig. S7c and S7f), the $Li^+$ diffusivity ( $D_{Li^+}$ ) can be calculated by Fick's second law, and the formula can be denoted as:[2]

$$D_{Li^+} = \frac{4}{\pi\tau}\left(\frac{mV_M}{MS}\right)^2\left(\frac{\Delta E_s}{\Delta E_t}\right)^2$$

where m, $M$ and $V_M$ represent the mass, the molar mass and the molar volume of SC622, respectively. Besides, $\tau$ is the time duration of the pulse, $S$ is the cell interfacial area, $\Delta E_s$ is the potential change at the state of equilibrium and $\Delta E_t$ is the total potential change.[3]

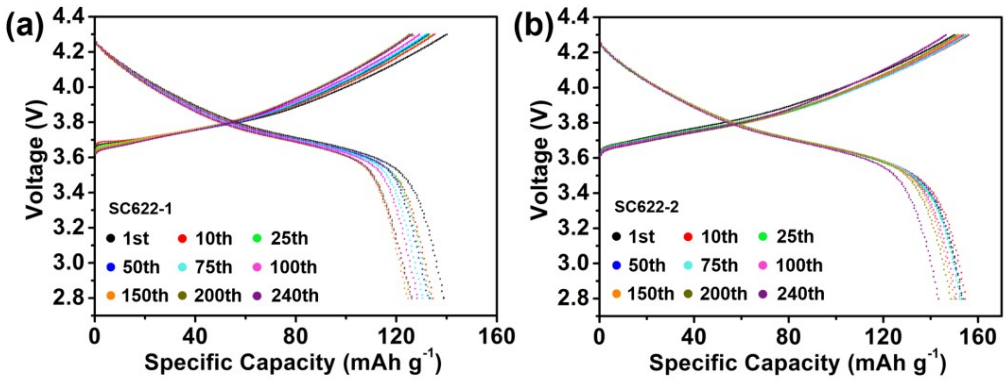


**Fig. S8.** Charge/discharge profiles of (a) SC622-1 and (b) SC622-2 at the 1st, 10th, 25th, 50th, 75th, 100th, 150th, 200th and 240th cycles.

The charge/discharge profiles of SC622-1 and SC622-2 are shown in Fig. S8. At a current rate of 1 C, SC622-2 electrode offers the better cycling performance than SC622-1. After 240 cycles, a high capacity of 146.2 mAh $g^{-1}$ can still be obtained for SC622-2, even higher than the initial capacity of SC622-1. In addition, there is no obvious change in the discharge plateau observed for SC622-1 and SC622-2, which indicates their capacity decays slowly.

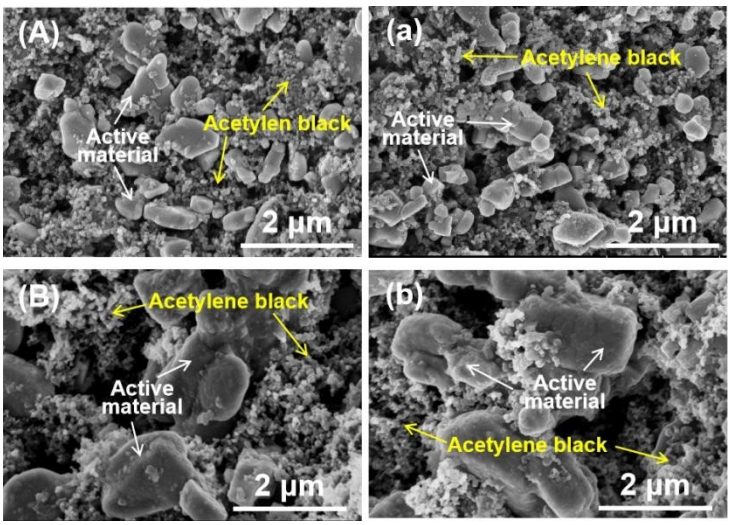


**Fig. S9.** *Ex-situ* FESEM images of the SC622-1 and SC622-2 electrodes (A-B) before and (a-b) after 240 cycles at 1 C, respectively.

*Ex-situ* FESEM images (Fig. S9) present that the large single-crystal particles of SC622-1 and SC622-2 are well sustained after cycling for 240 cycles at 1 C, claiming that the single crystal particle has high stability to resist particle fracture. In addition, the electrode also contains some particle fragments of acetylene black, which can be observed in the FESEM images of the electrode before and after cycling.

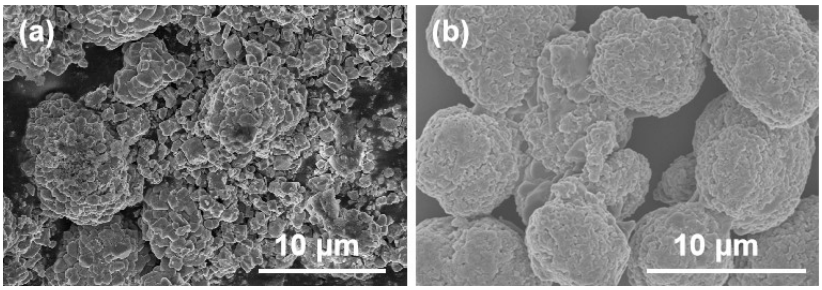


**Fig. S10.** FESEM images of (a) S523, (b) S811.

FESEM images of S523 (Fig. S10a) and S811 (Fig. S10b) indicate that the particle of S523 has been pulverized, while S811 is spherical particle.

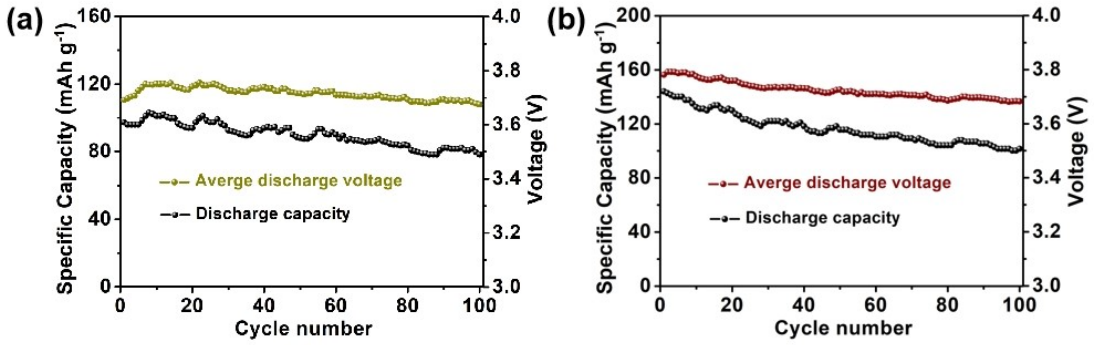


**Fig. S11.** Cycling performance and corresponding average discharge voltage of (a) S523, (b) S811 at 1 C.

The cycling performances and the corresponding average discharge voltage of S523 and S811 are displayed in Fig. S11. Cycling performance tests show that both the S523 and S811 perform poorly. For S523, the initial capacity is 97.2 mAh $g^{-1}$, with 80.6% capacity retention after 100 cycles. For S811, the initial capacity is 144.0 mAh $g^{-1}$, with 70.6% capacity retention after 100 cycles. In addition, the average discharge voltage of both materials declines greatly, indicating poor stability of the two materials.

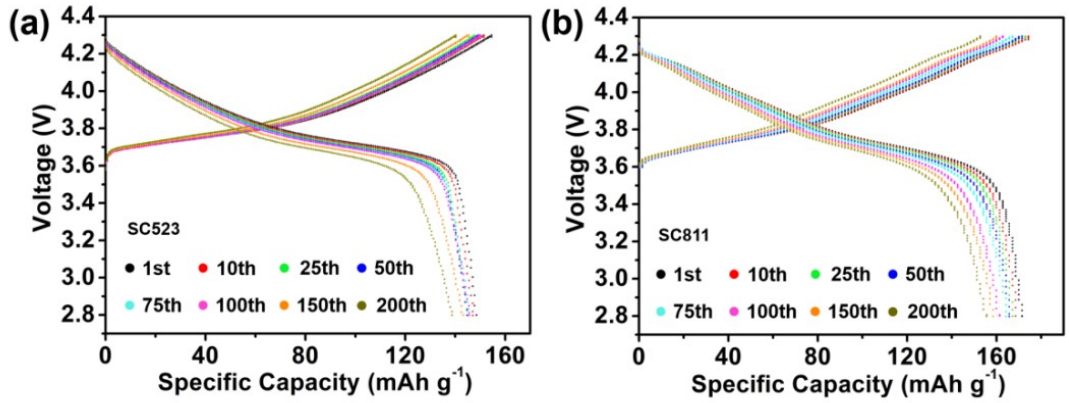


**Fig. S12.** Charge/discharge profiles of (a) SC523, (b) SC811 at the 1st, 10th, 25th, 50th, 75th, 100th, 150th, and 200th cycles.

The charge/discharge profiles of SC523 and SC811 are shown in Fig. S12. After cycling for 200 cycles at 1 C, the SC523 (Fig. S12a) presents a high capacity of 138.8 mAh $g^{-1}$, while SC811 (Fig. S12b) delivers a capacity of 148.3 mAh $g^{-1}$ but exhibits a little faster discharge plateau decrease with cycling than the SC523.

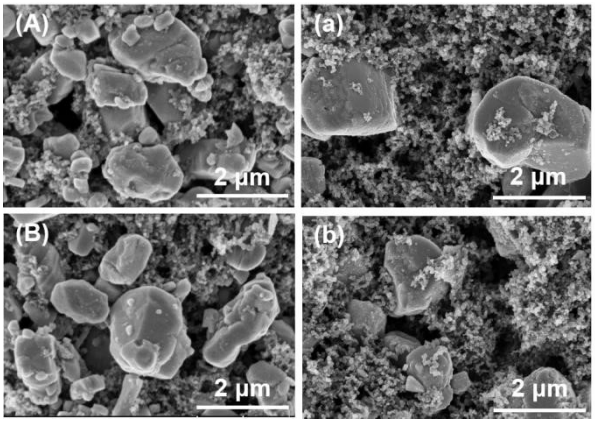


**Fig. S13.** *Ex-situ* FESEM images of the SC523 and SC811 electrodes (A-B) before and (a-b) after 200 cycles at 1 C, respectively.

*Ex-situ* FESEM images (Fig. S13) present that the single-crystal particles of SC523 and SC811 are well sustained after cycling for 200 cycles at 1 C.

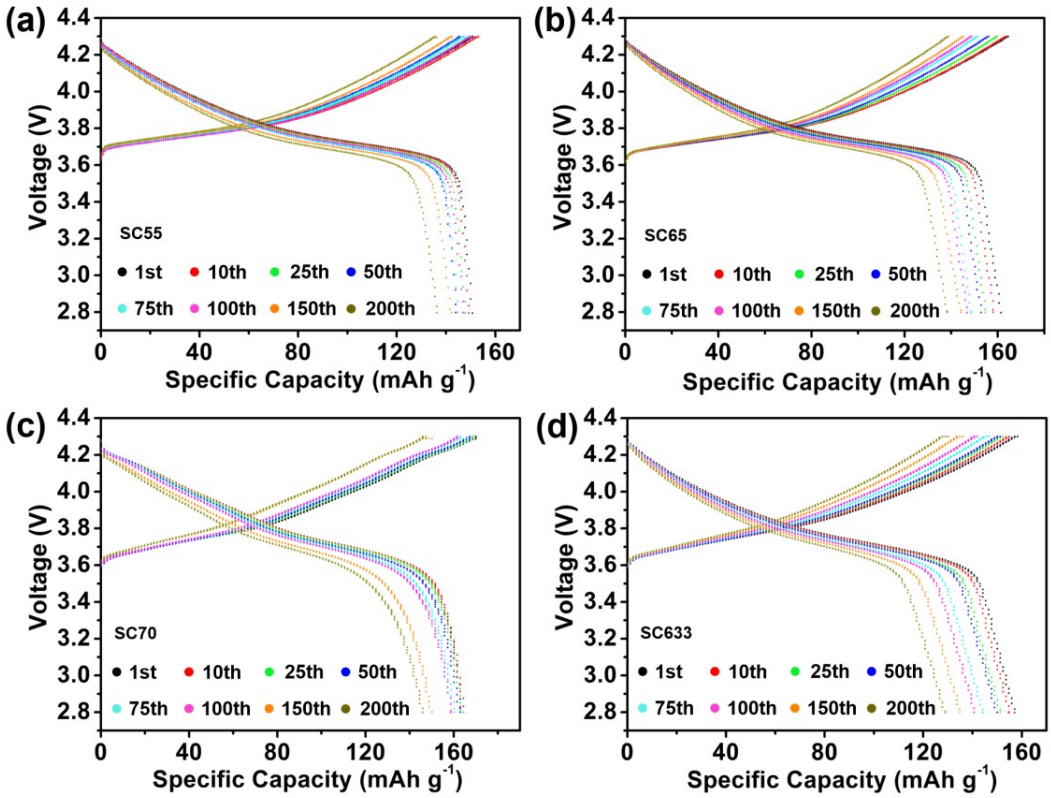


**Fig. S14.** Charge/discharge profiles of (a) SC55, (b) SC65, (c) SC70, and (d) SC633 at the 1st, 10th, 25th, 50th, 75th, 100th, 150th, and 200th cycles.

The charge/discharge profiles of SC55, SC65, SC70 and SC633 are shown in Fig. S14. After cycling for 200 cycles at 1 C, the capacity is 137.7 mAh $g^{-1}$ for SC55 (Fig. S14a), 138.1 mAh $g^{-1}$ for SC65 (Fig. S14b), 145.9 mAh $g^{-1}$ for SC70 (Fig. S14c), and 128.8 mAh $g^{-1}$ for SC633 (Fig. S14d). The capacity retention is 90.4%, 85.6%, 88.8%, and 82.0% for SC55, SC65, SC70, and SC633, respectively.

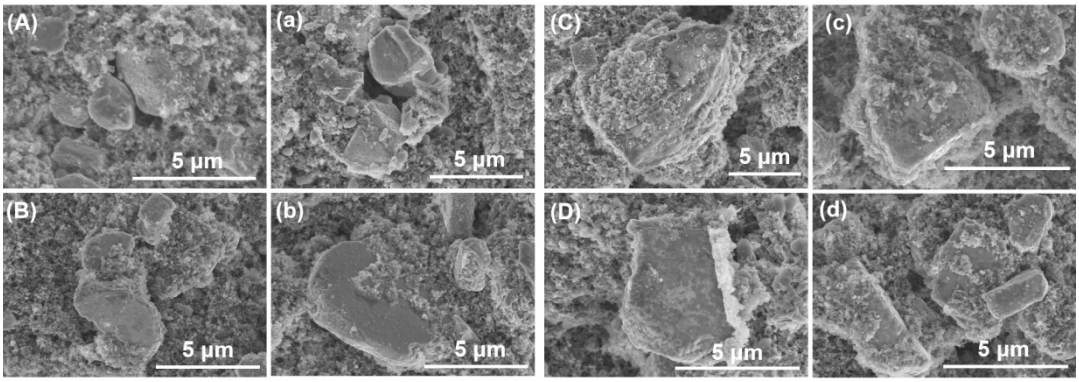


**Fig. S15.** *Ex-situ* FESEM images of the SC55, SC65, SC70, and SC633 electrodes (A-D) before and (a-d) after 200 cycles at 1 C, respectively.

*Ex-situ* FESEM images (Fig. S15) declare that all of these single-crystal particles of SC55, SC65, SC70, and SC633 samples are well preserved after cycling for 200 cycles at 1 C.

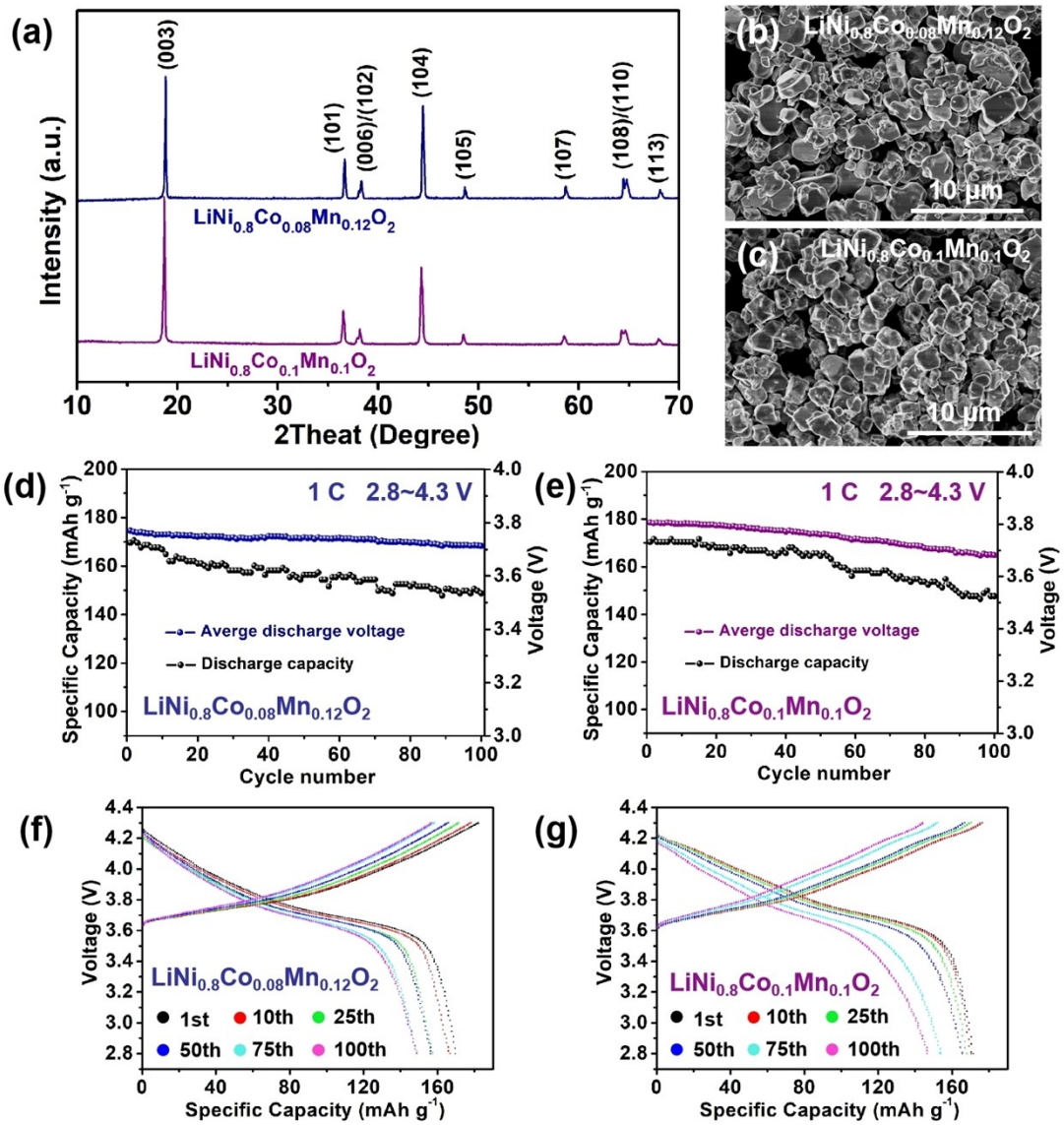


**Fig. S16.** (a) XRD patterns of single-crystal $LiNi_{0.8}Co_{0.08}Mn_{0.12}O_2$ and single-crystal $LiNi_{0.8}Co_{0.1}Mn_{0.1}O_2$. FESEM images of (b) single-crystal $LiNi_{0.8}Co_{0.08}Mn_{0.12}O_2$ and (c) single-crystal $LiNi_{0.8}Co_{0.1}Mn_{0.1}O_2$. The cycling performance and the average discharge voltage at 1 C of (d) single-crystal $LiNi_{0.8}Co_{0.08}Mn_{0.12}O_2$ and (e) single-crystal $LiNi_{0.8}Co_{0.1}Mn_{0.1}O_2$. Charge/discharge profiles of (f) single-crystal $LiNi_{0.8}Co_{0.08}Mn_{0.12}O_2$ and (g) single-crystal $LiNi_{0.8}Co_{0.1}Mn_{0.1}O_2$ at the 1st, 10th, 25th, 50th, 75th, and 100th cycles.

As shown in Fig. S16a-c, the $LiNi_{0.8}Co_{0.08}Mn_{0.12}O_2$ and $LiNi_{0.8}Co_{0.1}Mn_{0.1}O_2$

samples exist in micro-sized single-crystal particles with well-layered structure. Further cycling performance showed that the capacity retention rates were 87.7% for single-crystal $LiNi_{0.8}Co_{0.08}Mn_{0.12}O_2$ and 86.6% for single-crystal $LiNi_{0.8}Co_{0.1}Mn_{0.1}O_2$ after 100 cycles at 1 C (Fig. S16d,e). The corresponding charge/discharge curves of single-crystal $LiNi_{0.8}Co_{0.08}Mn_{0.12}O_2$ and single-crystal $LiNi_{0.8}Co_{0.1}Mn_{0.1}O_2$ display a gradual capacity decay (Fig. S16f,g). Therefore, the molten salt strategy is very proficient in regenerating spent NCM523 or spent NCM622 into micro-sized single-crystal $LiNi_xCo_yMn_zO_2$ cathode materials with a targeted Ni content of 80% by supplementing extra Ni source to react with them.

**Table S1.** Results of ICP-MS for S622, SC622-1, and SC622-2.

| Samples | Measured atomic ratio |
|---|---|
| S622 | Li:Ni:Co:Mn=0.783:0.600:0.205:0.198 |
| SC622-1 | Li:Ni:Co:Mn=1.013:0.600:0.199:0.193 |
| SC622-2 | Li:Ni:Co:Mn=1.034:0.600:0.207:0.203 |

**Table S2.** The relative ratio of $Ni^{2+}$ and $Ni^{3+}$ in the samples.

| Samples | The relative ratio of $Ni^{2+}$ | The relative ratio of $Ni^{3+}$ |
|---|---|---|
| S622 | 66.9% | 33.1% |
| SC622-1 | 44.5% | 55.5% |
| SC622-2 | 42.8% | 57.2% |

**Table S3.** Results of ICP-MS for S523, SC523, S811, SC811, SC55, SC65, SC70 and SC633.

| Samples | Measured atomic ratio |
|---|---|
| S523 | Li:Ni:Co:Mn=0.815:0.500:0.198:0.304 |
| SC523 | Li:Ni:Co:Mn=1.041:0.500:0.197:0.299 |
| S811 | Li:Ni:Co:Mn=1.054:0.800:0.103:0.107 |
| SC811 | Li:Ni:Co:Mn=1.032:0.800:0.106:0.105 |
| SC55 | Li:Ni:Co:Mn=1.056:0.550:0.203:0.258 |
| SC65 | Li:Ni:Co:Mn=1.105:0.650:0.157:0.196 |
| SC70 | Li:Ni:Co:Mn=1.029:0.700:0.144:0.153 |
| SC633 | Li:Ni:Co:Mn=1.017:0.633:0.161:0.194 |

## References


1 F. Xiong, Z. Chen, C. Huang, T. Wang, W. Zhang, Z. Yang, and F. Chen, Inorg. Chem., 2019, **58**, 15498−15506.

2 E. Markevich, M. D. Levi, and D. Aurbach, *J. Electroanal. Chem.* 2005, **580**, 231−237.

3 H. X. Zhang, Y. Liu, H. Jiang, Z. N. Deng, H. L. Liu, and C. Z. Li, *Chem. Eng. Sci.* 2019, **207**, 611−618.